Paper Template for 13th International Conference on Fracture

FirstName LastName[1,*], Second Author[1], Third Author[2]

Cracking simulation of ceramic materials under thermal shock by a non-local fracture model

Li Jia[1,*], Song Fan[2], Jiang Chiping[3]

[1]LSPM, CNRS UPR 3407, Université Paris XIII, Villetaneuse, France;
[2]State Key Laboratory of Nonlinear Mechanics, Institute of Mechanics, Chinese Academy of Sciences, Beijing, China;
[3]Solid Mechanics Research Center, Beijing University of Aeronautics and Astronautics, Beijing, China
[*]Corresponding author: jia.li@univ-paris13.fr

Abstract: In this work, we attempted to simulate the cracking process of ceramic beams subjected to quenching from different high temperatures to the ambient one. Based on a non-local damage theory and the linear fracture mechanics, a numerical model was established and implemented into a finite element code. This model is adjusted with two critical situations: it is equivalent to the maximum principal stress criterion when the specimen is subjected to uniform tensile stress and to the Griffith-Irwin criterion for the growth of a macro-crack. By using this numerical model, the initiation and propagation of cracks in quenched ceramic specimens were simulated. It was proved that the proposed damage model is capable to describe the detailed cracking process with high reliability comparing to the experimental results. Several typical characteristics in thermal shock failure such as the multi-cracking procedure, the hierarchical crack distribution, the distances between cracks etc. were faithfully described with high accuracy.

Key words: Thermal shock; Crack patterns; Non-local fracture model; Numerical simulations; Ceramics

1. Introduction

Ceramic materials exhibit excellent high temperature mechanical properties, corrosion resistance, wear resistance, erosion resistance, oxidation resistance etc. However, they are in general quite vulnerable to thermal shock failure. In general, crack formation is considered as the major reason of failure in thermo-structural engineering. Understanding the mechanisms of cracking process in ceramics under thermal loads has been one of the most importance tasks in the research of this field.

The earliest researches on fracture of ceramic materials underwent thermal shock by Kingery [1,2] and Hasselman [3]. Afterward, numerous theoretical and experimental studies on thermal shock failure of ceramics have been reported [4-15]. However, the crack pattern formation under thermal shock is quite a rapid and highly complicated process. This process is difficult to capture with available experimental techniques. Only final crack patterns can easily be observed. This is why direct numerical simulations are particularly interesting in reproducing the cracking process. As results, the failure mechanisms and the control parameters can be better understood. Unfortunately, the direct numerical simulations have rarely been reported in the literature so far due to the inherent complexities in multi-cracking modelling.

In this work, a non-local failure criterion was used and implemented into a finite element code and then applied to simulate the crack evolution in ceramic materials subjected to thermal shock. The proposed fracture model is equivalent to the maximum principal stress criterion for a specimen under pure tensile loading, and to the Griffith-Irwin criterion for the crack propagation. Consequently, this non-local fracture model can both predict crack initiation as well as crack

growth. The numerical simulations successfully reproduce the cracking patterns in ceramic specimens after quenching. The periodical and hierarchical characteristics of the crack patterns are predicted with satisfactory accuracy. Moreover, the direct numerical simulations faithfully describe whole the cracking process, including the crack initiation, crack growth and crack arrest during quenching tests. By comparing to the previous experimental results, the accuracy and efficiency of the proposed model are examined and discussed. Finally, we give some concluding remarks and directions to follow in future works.

2: Non-local damage model

We first outline briefly the non-local fracture model proposed in Li et al. [16-17]. The basic idea of this model consists in replacing the local damage driving force, an effective stress σ_e for example, by its weighted average over a representative volume V [18]:

$$\widetilde{\sigma}_e(\mathbf{x}) = \frac{1}{\int_V \alpha(\mathbf{x}-\mathbf{y})d\mathbf{y}} \int_V \alpha(\mathbf{x}-\mathbf{y})\sigma_e(\mathbf{y})d\mathbf{y} \tag{1}$$

where α is a weighting function. In the present work, a cone-shape function is adopted for simplicity:

$$\alpha(r) = \begin{cases} 0 & r > R \\ 1-\dfrac{r}{R} & r \le R \end{cases} \tag{2}$$

where $r = \|\mathbf{x}-\mathbf{y}\|$; R is the radius of non-local action, representing a material characteristic length which defines the size of interaction zone in failure process.

We assume reasonably that the failure in ceramic materials under uniform stress fields obeys the maximum principal stress criterion. However, it can not directly be utilized to predict crack growth due to the stress singularity near the crack tips. This shorthand can be overcome by a non-local formulation such like Eq. (1). Thus, the non-local maximum principal stress criterion can be written as follows:

$$D = \begin{cases} 0 & \widetilde{\sigma}_1 < \sigma_c \\ 1 & \widetilde{\sigma}_1 \ge \sigma_c \end{cases} \tag{3}$$

where D is the damage, σ_c is the ultimate stress of the material, $\widetilde{\sigma}_1$ is the non-local first principal stress. We enforce the validity of criterion (3) in two special cases: First, it should be valid in the case of a uniform tensile load. It is clear that this condition is automatically satisfied since in this case, we have $\widetilde{\sigma}_1 = \sigma_1$. Second, it should be valid for the growth of a mode-I crack. To this end, we assume that the near-tip stress field is governed by the Williams asymptotic expansion [19]. Therefore, for a mode-I loaded crack, the non-local first principal stress near the crack tip writes, according to (1) and (2):

$$\widetilde{\sigma}_1(r,\theta)=\frac{1}{\int_0^R\int_{-\pi}^{\pi}\left(1-\frac{r'}{R}\right)r'dr'd\theta'}\int_0^R\int_{-\pi}^{\pi}\left(1-\frac{r'}{R}\right)\frac{K_I}{\sqrt{2\pi r}}\left(1+\cos\frac{\theta}{2}\right)\left|\sin\frac{\theta}{2}\right|r'dr'd\theta' \tag{4}$$

where K_I is the stress intensity factor, r and θ are the polar coordinates with the origin at the crack tip. Under mode I loading, the maximum non-local principal stress is located at a point on the crack axis near the crack tip $r=r_0,\theta=0$ due to the symmetry. We assume that r_0 is small such that the stress at its vicinity is still governed by the crack-tip asymptotic field. On the one hand, according to the damage criterion (3), the element at $(r=r_0,\theta=0)$ is broken when $\widetilde{\sigma}_1\geq\sigma_c$. On the other hand, from the Griffith-Irwin criterion of fracture [20-21], the crack grows when $K_I\geq K_{Ic}$, where K_{Ic} is the critical stress intensity factor. This condition permits us to determine the non-local action radius R by resolving numerically the following equation:

$$f(R)=\sigma_c-\max_{r_0}\int_0^R\int_{-\pi}^{\pi}\frac{3}{\pi R^2}\left(1-\frac{r'}{R}\right)\frac{K_{Ic}}{\sqrt{2\pi r}}\left(1+\cos\frac{\theta}{2}\right)\left|\sin\frac{\theta}{2}\right|r'dr'd\theta'=0 \tag{5}$$

with

$$r=\sqrt{(r_0+r'\cos\theta')^2+(r'\sin\theta')^2}\quad\tan\theta=\frac{r'\sin\theta'}{r_0+r'\cos\theta'}$$

Thus, the non-local damage criterion (3) is exactly equivalent to Griffith-Irwin criterion when the non-local action radius R is determined by (5). Consequently, we can confirm that in the cases of uniform tensile loads and mode-I cracks, the fracture can exactly be predicted by using the criterion (3). From this point of view, the proposed non-local criterion can be used to predict the crack initiation as well as the crack propagation. In practice, we just need to find the point where the non-local principal stress is maximal: this point is broken when the non-local stress attaints the material strength.

The proposed non-local fracture criterion was implemented into a finite element code. As the criterion (3) is an instantaneous damage model, an element is linearly elastic before its complete failure. Therefore, the crack propagation prediction is very similar to that adopted in the linear elastic fracture mechanics: A linear elastic calculation is first carried out for the cracked structure; then the crack propagation is determined according to a suitable criterion. This procedure is then repeated after each small crack progression in the structure. In the present work, the crack propagation is represented by successive eliminations of groups of damaged elements.

3. Thermal shock problem

The proposed non-local criterion was used to evaluate the cracking process in ceramic specimens under thermal shock.

3.1 Experiments

Jiang et al. [14] carried out quenching experiments on ceramics plates from different temperatures. This experimental study will be used in the validation of the proposed model. In Jiang et al. [14], 99% Al_2O_3 powder was thermoformed into 50mm×10mm×1mm thin specimens. They were bound up with inconel wires and heated to a temperature T_0 ranged from 300°C to 600°C. After that, the heated specimens were dropped into a water bath of T_∞=20°C by free fall. Figure 1 shows the thermal shock crack patterns. From Figure 1, we can remark the following points:

- The number of cracks increases as the initial temperature increases;
- The lengths of the cracks increase as the initial temperature increases;
- The crack spacing decreases as the initial temperature increases;
- A tendency towards equal spacing between cracks can be observed;
- The crack patterns exhibit a hierarchical structure. One can distinguish 2 classes' cracks for quenching tests with T_0=300°C, and 3 classes' cracks for quenching tests with T_0=350°C ~ 600°C. However, the frontiers of the different classes are not always clear.

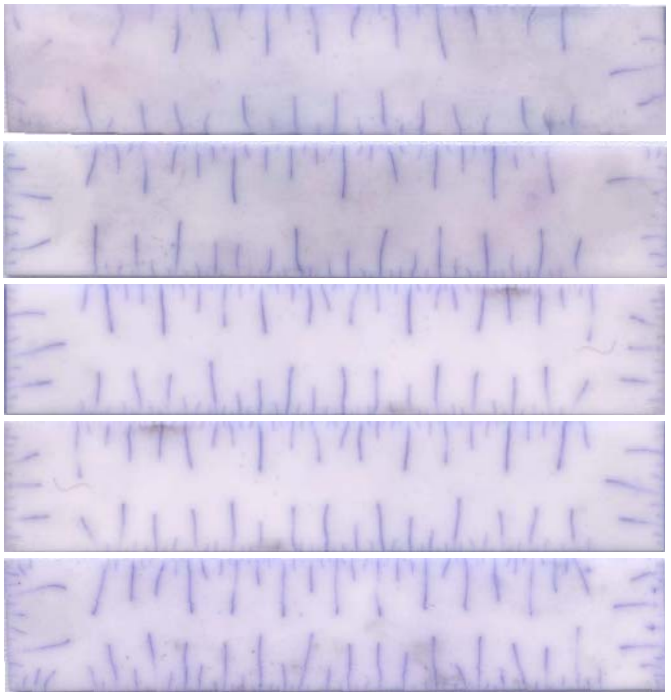

Figure 1: Crack patterns after quenching experiments

3.2 Model

By considering the symmetry of the specimen, a quart of it was meshed by using three-node plane stress elements. The side size of the elements is about d= 0.05mm, e.g. about a half of the non-local action radius R. When the failure criterion is fulfilled in an element, it will be eliminated from the model, together with its immediate neighbouring elements. The successive damaged spots form a damaged band with a width of about 0.12mm.

3.3 Temperature and thermal stress fields

The experimental conditions allow us to regard the temperature field as two-dimensional. Establish a Cartesian coordinate system Oxy with the origin at the centre of the specimen and x and y

coinciding with the specimen axes. Noting that during the process of water quenching, the water temperature holds at T_∞=20°C in the bath. According to the thermal transfer calculation, the temperature distribution at any instant in the specimen writes:

$$\frac{T}{T_0}=\left[\sum_{m=1}^{\infty}X_m\exp\left(-\alpha_m^2\frac{at}{L_1^2}\right)\cos\left(\alpha_m\frac{x}{L_1}\right)\right]\left[\sum_{m=1}^{\infty}Y_m\exp\left(-\beta_m^2\frac{at}{L_2^2}\right)\cos\left(\beta_m\frac{y}{L_2}\right)\right] \quad (6)$$

where t is the time, $a=k/\rho c$; k, ρ, c are the thermal conductivity, density and specific heat, respectively; T_0 is the initial temperature assumed to be uniform in the specimen; and

$$X_m=\frac{2\sin\alpha_m}{\alpha_m+\sin\alpha_m\cos\alpha_m} \quad Y_m=\frac{2\sin\beta_m}{\beta_m+\sin\beta_m\cos\beta_m}$$

with α_m and β_m are the roots of the following transcendent equations:

$$\tan\alpha_m=\frac{hL_1}{k\alpha_m} \quad \tan\beta_m=\frac{hL_2}{k\beta_m}$$

where L_1 and L_2 are respectively the semi-length and semi-width of the specimen; h is the convective heat transfer coefficient.

3.4: Material parameters

The ceramic specimens were assumed to be linearly elastic, homogeneous and isotropic. From available data, Young's modulus E, Poisson's ratio ν, the ultimate tensile stress σ_c, the density ρ [22], and the energy release rate G [23] of 99% Al_2O_3 ceramics are listed in Table 1. The critical stress intensity factor is deduced from $K_{Ic}=\sqrt{GE}$. The non-local action radius deduced from (5) is R=0.1176mm. Conversely, the thermal parameters such like the thermal conductivity k, the specific heat c and the thermal expansion coefficient α are temperature-dependent [24-26]. Consequently, adopting constant values in the quenching simulations is an approximate and simplified assumption. The values used in the simulations are taken from [24-26] and also listed in Table 1. The available data [27-30] on the convective heat transfer coefficient h in thermal shock give scattering estimations ($h \approx 10^4$~10^5W/(m^2·K)). In this work, a constant value for h was used in all the simulations, its value was estimated such that the numerical results on average crack spacing at each quenching temperature approximately agree with the experimental measurement. The value used in the present work is h =50000W/(m^2·K).

Table 1: Mechanical and thermal parameters used in the simulations

E(MPa)	ν	σ_c(MPa)	ρ(kg/m^3)
370000	0.3	180	3980;
G(J/m^2)	k(W/(m.K))	c(J/(kg.K))	α
24.3	31	880	7.5×10^{-6}

4. Results and discussions

4.1: Direct comparison with the experiments

Figure 2 illustrates the final crack patterns of the simulations for different initial quenching temperature. For comparison, the experimentally obtained crack patterns are also showed. Globally speaking, the simulations reproduce faithfully the crack patterns obtained from quenching tests. The resemblance between the numerical results and the real tests is obvious. Following remarks can be made:

1. As in quenching tests, multi-cracking patterns are obtained;
2. As in quenching tests, the cracks can be classified into 2 or 3 hierarchical levels;
3. As in quenching tests, the tendency towards equal crack spacing is obvious.

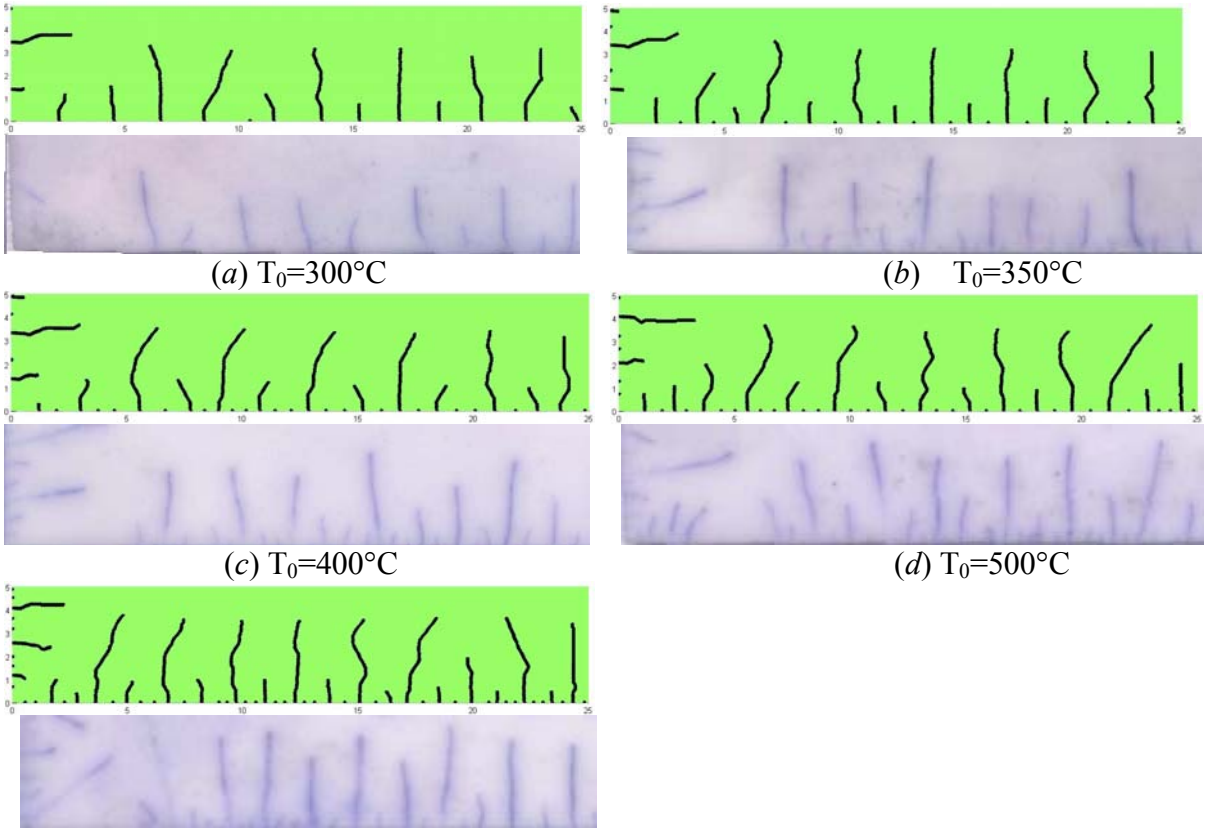

(*a*) T_0=300°C (*b*) T_0=350°C

(*c*) T_0=400°C (*d*) T_0=500°C

(*e*) T_0=600°C

Figure 2: Comparison between the crack patterns in numerical models and in real specimens

4.2: Characteristic values of the crack patterns

Statistically speaking, the principal features of the crack patterns can be brought out from numerical results. Table 2 shows the comparison between the experimental and numerical results on average crack spacing *s* observed at the specimen surfaces. From this comparison, we can see the numerical simulations are quite accurate, even by using constant material parameters.

Table 2: Dimensionless average crack spacing $\bar{s} = s/L_2$

T_0	300°C		350°C		400°C		500°C		600°C	
	test	simulation	test	simulation	test	Simulation	test	simulation	test	simulation
$\bar{s}$	0.32	0.333	0.184	0.181	0.16	0.158	0.142	0.133	0.12	0.105

Although the morphologies are very similar between the experimental crack patterns and the numerical ones, the quantitative comparison on crack lengths p is not evident due to the data scattering of the experimental results. By assuming that each crack level obeys a Gaussian distribution, Jiang et al. [14] described the crack length distribution by a combined Gaussian function. This analysis allowed the classification of the cracks according to their length in a statistical manner. In Table 2, we list the average lengths of the longest cracks of the experimental and numerical crack patterns. The comparison shows a good agreement, even though the numerical simulations provide smaller crack lengths comparing to the experiments.
The principal reason of this difference may be the blunt form of the crack tips in numerical models, in which the cracks were represented by damaged bands with a finite thickness.

Table 3: Dimensionless crack length $\bar{p} = p/L_2$

T_0	300°C		350°C		400°C		500°C		600°C	
	test	simulation	Test	simulation	test	simulation	Test	simulation	test	simulation
$\bar{p}$	0.72	0.64	0.74	0.65	0.72	0.68	0.78	0.73	0.8	0.75

4.3: Cracking process during the thermal shock

Figure 3 shows the first crack initiations at the specimen surface. The distribution of the first principal stresses is also shown by means of a colouring map. From this image, we can observe that, at a critical time where the temperature gradient reaches a sufficiently high level, the first crack will appear at the location where the non-local first principal stress is maximal and fulfils the failure criterion (3). After that, the stresses are relaxed at this location, and the stress redistribution furnishes another location where the first principal stress is maximal. If the fracture criterion (3) is always fulfilled, a new crack onset takes place. Since the stress distribution is nearly uniform along the specimen surface, the first crack initiations are somewhat randomly located, depending only on the scattering of the numerical results. The following cracks will appear between the most distant cracks previously formed. This procedure will repeat until the temperature gradient is no longer capable to produce sufficient stress concentration to onset new cracks.

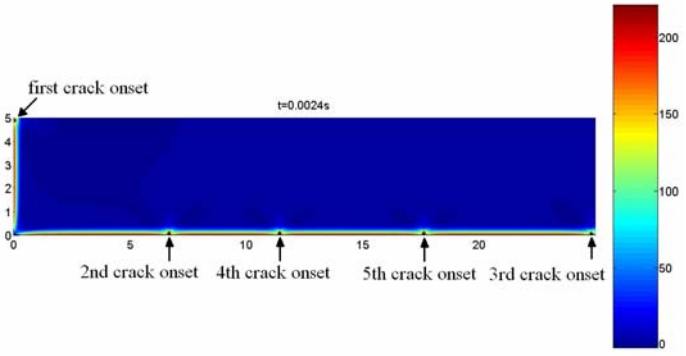

Figure 3: First crack initiations

Figure 4 shows some different steps of the cracking process. The crack growth scheme can be summarized by observing these images. At the beginning, the thermal shock cracks initiate and propagate uniformly with approximately a nearly equal spacing (Fig. 4-*a*). At this step, the thermal shock cracks propagate simultaneously and very rapidly, then the propagation speed decreases gradually with release of the thermal stresses until the strain energy cannot support simultaneous propagation of all the cracks. Consequently, only a reduced number of cracks continue to propagate, whereas the other cracks stop. The crack spacing increases until 2 or 3 times larger than the previous one (Fig. 4-*b*). In the following steps, the crack growth may deviate and attempt to form equal crack spacing (Fig. 4-*c*). This procedure may repeat several times until the strain energy induced by thermal stresses cannot support propagation of any crack. The final simulation crack patterns (Fig. 4-*d*) are very similar to those observed in experimental results. This remark supports the cracking process above described.

The colouring map represents the levels of first principal stresses (unity in MPa). From Figure 4, the locations of stress concentrations can clearly be observed. The competition amongst the stress concentrations at different locations leads to the formation of multi-crack failure patterns. The proposed damage model provides a natural manner in reproducing them. Comparing to the traditional treatment of fracture mechanics in which the crack growth conditions should be examined at each crack tip, the present method is much more simple and robust to deal with multi-cracking problems.

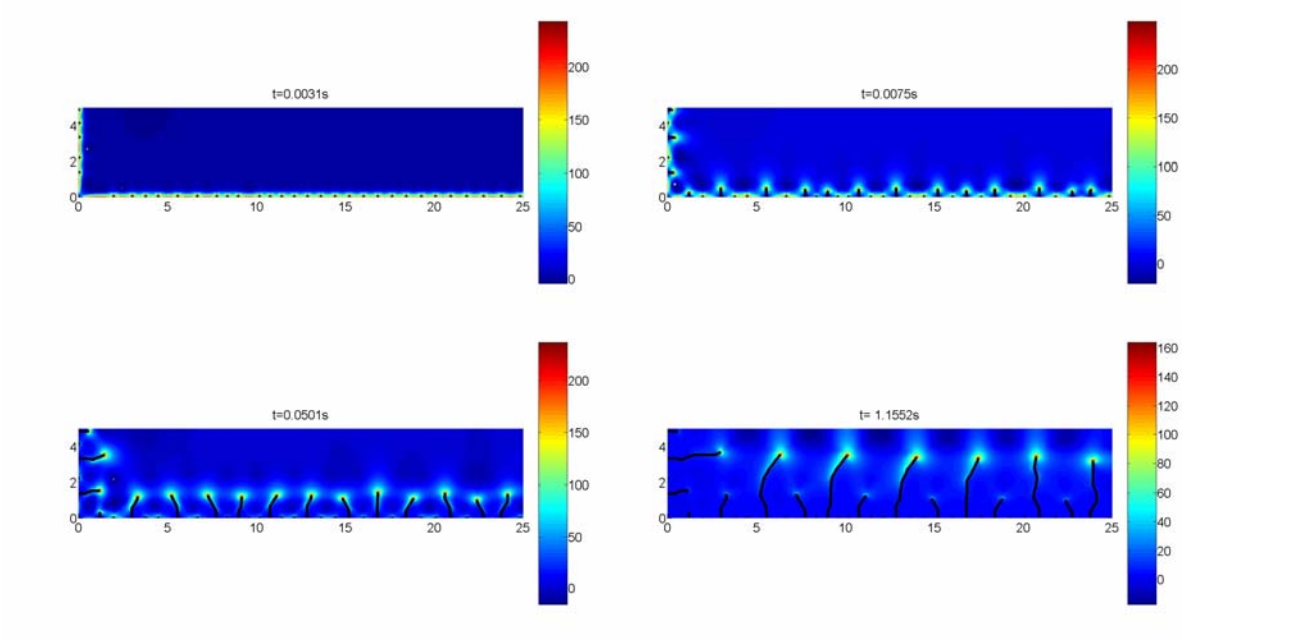

Figure 4: Crack patterns at different times, T_0=500°C

5. Conclusions and future works

In this work, a non-local failure model was described to predict crack initiation and crack growth in brittle materials and then implemented into a finite element code. This non-local fracture model was

successfully applied to simulating the crack evolution in ceramic materials subjected to thermal shock. From the results of the numerical simulations, the following conclusions can be formulated:

1. The numerical simulations reproduced faithfully the crack patterns in ceramic specimens after quenching tests. The periodical and hierarchical characteristics of the crack patterns were accurately predicted;
2. The parameters describing the crack patterns such as the average crack spacing and the crack lengths were correctly estimated from the numerical results;
3. The numerical simulations allow a direct observation on crack initiation and growth in the specimens, which is quite a difficult task in experimental studies.
4. The finite element implementation of the proposed non-local criterion allows accurate cracking simulations for real structures under thermal shock. The theoretical concept is clear and simple. The numerical model is robust, easy to apply to different engineering structures subjected to thermal shock.

Acknowledgements

This work was supported by the funding from the French ANR program T-Shock ANR-10-INTB-0915 and the National Natural Science Foundations of China (Grants Nos. 11061130550 and 11172023).

References

[1] W. D. Kingery, Metal-ceramic interaction: IV, absolute measurement of metal-ceramic interfacial energy and interfacial adsorption of silicon from iron-silicon alloys,
J. Am. Ceram. Soc., 1954, 37: 42~25.

[2] W.D. Kingery, Factors affecting thermal stress resistance of ceramic materials, J. Am. Ceram. Soc., 1955, 38: 3~15.

[3] D.P.H. Hasselman, Approximate theory of thermal stress resistance of brittle ceramics involving creep, J. Am. Ceram. Soc., 1969, 50: 454~457.

[4]. Mai, Y. W., Thermal stress resistance and fracture toughness of two tools ceramics. J. Mat. Sc., 1976, 11, 1430–1438.

[5]. Hasselman, D. P. H., Strength behaviour of polycristalline alumina subjected to thermal shock. J. Am. Ceram. Soc., 1970, 53(9), 490–495.

[6]. Ziegler, G. and Heinrich, J., Effect of porosity on the thermal shock behaviour of reaction sintered silicon nitride. Ceramurgia Inter., 1980, 6(1), 25–30.

[7] T.K. Gupta, Strength degradation and crack propagation in thermally shocked alumina, J. Am. C eram. Soc., 1972, 55(5): 249~253.

[8] J.A. Coppola, D.P.H. Hasslman, Strength loss of brittle ceramics subjected to severe thermal sho ck, J. Am. Ceram. Soc., 1972, 55(9): 481~489.

[9] T. J. LU and N. A. FLECK, THE THERMAL SHOCK RESISTANCE OF SOLIDS
, Acta mater. Vol. 46, No. 13, pp. 4755-4768, 1998

[10] Bažant ZP, Ohtsubo H, Aoh K. Stability and post-critical growth of a system of cooling or shrinkage cracks. Int J Fract 1979; 15(5): 443-456.

[11] Nemat-Nasser S, et al. Unstable growth of thermally induced interacting cracks in brittle solids.

Int J Solids Structures 1978; 14(6): 409-430.
[12] Bahr HA, Fischer G, Weiss HJ. Thermal-shock crack patterns explained by single and multiple crack propagation. J Mater Sci 1986; 21(8): 2716-2720.
[13] Hans-Achim Bahr, Hans-Jurgen Weiss, Ute Bahr, Martin Hofmann, Gottfried Fischer, Stefan Lampenscherf, Herbert Balke , Scaling behavior of thermal shock crack patterns and tunneling cracks driven by cooling or drying, Journal of the Mechanics and Physics of Solids 58 (2010) 1411–1421
[14] C.P. Jiang, X.F. Wu, J. Li , F. Song, Y.F. Shao, X.H. Xu, P. Yan, A study of the mechanism of formation and numerical simulations of crack patterns in ceramics subjected to thermal shock, Acta Materialia 60 (2012) 4540–4550
[15] B.Bourdin, J.-J. Marigo, C. Maurini, The variational approach to fracture mechanics: application to numerical simulation of thermal-shock cracks, IV European Conference on Computational Mechanics (ECCM2010), 16-21 May 2010 Paris, France.
[16] Li Jia, Tian Xiao Xiao, Abdelmoula Radhi, A damage model for crack prediction in brittle and quasi-brittle materials solved by the FFT method, International Journal of Fracture, 2012, Vol 173:135–146
[17] Li Jia, Meng Songhe, Tian Xiao Xiao, Song Fan, Jiang Chiping, A non-local fracture model for composite laminates and numerical simulations by the FFT method, Composites, Part B 43 (2012) 961–971
[18] Pijaudier-Cabot G, Bazant ZP. Nonlocal damage theory. J Engng Mechanics ASCE, 1987;113:1512-1533.
[19] Williams M.L. (1952), Stress singularities resulting from various boundary conditions in angular corners of plates in extension. ASME Journal of Applied Mechanics, 19,526-528
[20] Griffith AA. The phenomena of rupture and flow in solids. Philosophical Transactions of the Royal Society of London, 1920;221:163–198
[21] Irwin G. Linear fracture mechanics, fracture transition and fracture control, Eng. Fract. Mech., 1968;1:241-257
[22] Zhang YL, Ma JP. Applicable Ceramic Material Manual. Beijing: Chemical Industry Press; 2006. (in Chinese)
[24] Zhang QC. Mechanical Properties of Ceramics. Beijing: Science Press; 1987. (in Chinese)
[25] Touloukian YS, Ho CY. Thermophysical properties of matter. Thermal conductivity of nonmetallic solids, vol. 2. New York: Plenum Press; 1972.
[26] Touloukian YS, Ho CY. Thermophysical properties of matter. Specific heat of nonmetallic solids, vol. 5. New York: Plenum Press; 1972.
[27] Jiang DL et al. China materials engineering canon. Beijing: Chemical Industry Press; 2006 [in Chinese].
[28] Becher PF. Effect of water bath temperature on the thermal shock of Al_2O_3. J Am Ceram Soc 1981; 64(1): C-17-C-18.
[29] Kim Y, Lee WJ, Case ED. The measurement of the surface heat transfer coefficient for ceramics quenched into a water bath. Mater Sci Eng A 1991; 145(1): L7-L11.
[30] Zhou ZL, Song F, Shao YF, Meng SH, Jiang CP, Li J, Characteristics of the surface heat transfer coefficient for Al2O3 ceramic in water quench, *J Europ Ceram Soc* 2012 ; 32 : 3029–3034